Tumors in von Hippel–Lindau Syndrome: From Head to Toe—Comprehensive State-of-the-Art Review[1]

Dhakshinamoorthy Ganeshan, MD
Christine O. Menias, MD
Perry J. Pickhardt, MD
Kumaresan Sandrasegaran, MD
Meghan G. Lubner, MD
Preetha Ramalingam, MD
Sanjeev Bhalla, MD

Abbreviations: CNS = central nervous system, HB = hemangioblastoma, H-E = hematoxylin-eosin, NET = neuroendocrine tumor, RCC = renal cell carcinoma, VHL = von Hippel–Lindau syndrome, WHO = World Health Organization

RadioGraphics 2018; 38:849–866

https://doi.org/10.1148/rg.2018170156

Content Codes: CT GI GU MI MR NR

[1]From the Departments of Radiology (D.G.) and Pathology (P.R.), University of Texas MD Anderson Cancer Center, Pickens Academic Tower, 1400 Pressler St, Unit 1473, Houston, TX 77030-4009; Department of Radiology, Mayo Clinic Arizona, Phoenix/Scottsdale, Ariz (C.O.M.); Department of Radiology, University of Wisconsin School of Medicine and Public Health, Madison, Wis (P.J.P., M.G.L.); Department of Radiology, Indiana University School of Medicine, Indianapolis, Ind (K.S.); and Section of Abdominal Imaging, Mallinckrodt Institute of Radiology, Washington University School of Medicine, St Louis, Mo (S.B.). Recipient of a Certificate of Merit award for an education exhibit at the 2016 RSNA Annual Meeting. Received June 5, 2017; revision requested August 25 and received September 15; accepted October 30. For this journal-based SA-CME activity, the authors P.J.P. and M.G.L. have provided disclosures (see end of article); all other authors, the editor, and the reviewers have disclosed no relevant relationships. **Address correspondence to** D.G. (e-mail: *dganeshan@mdanderson.org*).

SA-CME LEARNING OBJECTIVES

After completing this journal-based SA-CME activity, participants will be able to:

- Describe the molecular cytogenetics and clinical manifestations of VHL.
- Identify characteristic multimodality imaging features of tumors in VHL that affect multiple organ systems.
- Discuss the latest advances in management of VHL and current recommendations for surveillance and screening.

See www.rsna.org/education/search/RG.

Von Hippel–Lindau syndrome (VHL) is an autosomal-dominant hereditary tumor disease that arises owing to germline mutations in the *VHL* gene, located on the short arm of chromosome 3. Patients with VHL may develop multiple benign and malignant tumors involving various organ systems, including retinal hemangioblastomas (HBs), central nervous system (CNS) HBs, endolymphatic sac tumors, pancreatic neuroendocrine tumors, pancreatic cystadenomas, pancreatic cysts, clear cell renal cell carcinomas, renal cysts, pheochromocytomas, paragangliomas, and epididymal and broad ligament cystadenomas. The VHL/hypoxia-inducible factor pathway is believed to play a key role in the pathogenesis of VHL-related tumors. The diagnosis of VHL can be made clinically when the characteristic clinical history and findings have manifested, such as the presence of two or more CNS HBs. Genetic testing for heterozygous germline *VHL* mutation may also be used to confirm the diagnosis of VHL. Imaging plays an important role in the diagnosis and surveillance of patients with VHL. Familiarity with the clinical and imaging manifestations of the various VHL-related tumors is important for early detection and guiding appropriate management. The purpose of this article is to discuss the molecular cytogenetics and clinical manifestations of VHL, review the characteristic multimodality imaging features of the various VHL-related tumors affecting multiple organ systems, and discuss the latest advances in management of VHL, including current recommendations for surveillance and screening.

Introduction

Von Hippel–Lindau syndrome (VHL) is a hereditary tumor syndrome, arising owing to germline mutations in the *VHL* tumor suppressor gene, located on the short arm of chromosome 3. VHL is an autosomal dominant disorder, with a prevalence of around one in 36 000 and one in 50 000 live births (1,2). Around 80% of patients with VHL inherit the disorder from an affected parent, while it may arise de novo in 20% (3). The mean age of initial tumor diagnosis in VHL is 26 years (range, 1–70 years) (4).

VHL is a highly penetrant disease, with more than 90% of patients developing symptoms by 65 years of age (1,4,5). Patients may develop multiple benign and malignant tumors involving various organ systems, including retinal hemangioblastomas (HBs), central nervous system (CNS) HBs, endolymphatic sac tumors, pancreatic neuroendocrine tumors (NETs), pancreatic cystadenomas, pancreatic cysts, clear cell renal cell carcinomas (RCCs), renal cysts, pheochromocytomas, paragangliomas, and epididymal and broad ligament cystadenomas (Fig 1) (4). In this article, we review the molecular cytogenetics of VHL, discuss the characteristic multimodality imaging features of various VHL-associated tumors, and review the latest advances in the management of VHL, including surveillance and screening.

TEACHING POINTS

- Patients may develop multiple benign and malignant tumors involving various organ systems, including retinal HBs, CNS HBs, endolymphatic sac tumors, pancreatic NETs, pancreatic cystadenomas, pancreatic cysts, clear cell RCCs, renal cysts, pheochromocytomas, paragangliomas, and epididymal and broad ligament cystadenomas.
- The VHL/hypoxia-inducible factor pathway is believed to play a key role in the pathogenesis of VHL-related tumors.
- A CNS HB is the prototype tumor of VHL, which may occur in the cerebellum, brainstem, spinal cord, cauda equina, or supratentorial region. Craniospinal HB is the most common VHL-associated tumor, with a reported frequency of 60%–80%.
- When a cerebellar HB is identified, it is important to image the whole spinal cord, as lesions in the spinal cord frequently coexist with cerebellar lesions.
- At CT, endolymphatic sac tumors may demonstrate a moth-eaten appearance in the petrous temporal bone, with erosive changes in the vestibular aqueduct, semicircular canals, and cochlea.

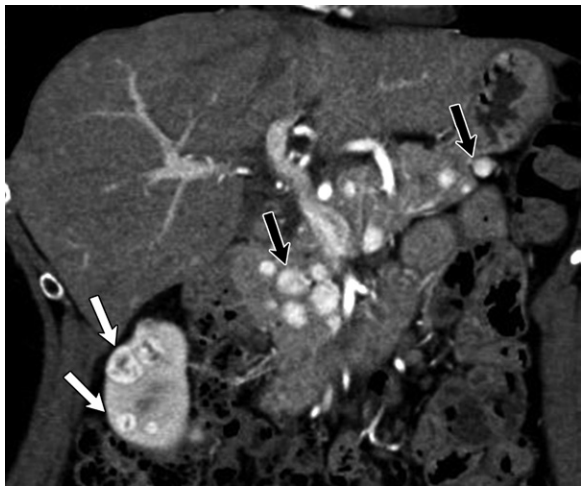

Figure 1. Multiple RCCs and pancreatic NETs in a 32-year-old man with VHL. Coronal computed tomographic (CT) image of the abdomen shows multiple heterogeneous avidly enhancing lesions (white arrows) in the right kidney and numerous scattered hypervascular masses (black arrows) in the pancreas.

Molecular Cytogenetics and Tumor Pathogenesis in VHL

Substantial advances have been made in the molecular cytogenetics of VHL, which have enhanced our understanding of the complex tumor biology of this condition. All patients with hereditary VHL inherit a single mutant defective allele from a germline *VHL* mutation. However, tumors develop in these patients only when a second somatic event affects the wild-type allele (Knudson "two-hit" hypothesis).

Missense mutations (27%–52%) are the most common type of germline mutations reported in VHL. However, a wide spectrum of germline mutations have been described, including frameshift mutations, nonsense mutations, large or microdeletions, gene rearrangements, in-frame deletions or insertions, and splice site mutations (6). Somatic inactivation of the wild-type allele may arise owing to allelic loss, hypermethylation, or point mutations (7).

VHL is a tumor suppressor gene located on chromosome 3p25–26. The protein derived from the *VHL* gene plays an important role in the hydroxylation of the hypoxia-inducible factor 1 alpha (HIF-α) under normoxic conditions. In VHL, the *VHL* gene becomes nonfunctional. Absence of the functional *VHL* gene leads to hyperaccumulation of HIF-α, which in turn can lead to excessive activation of numerous hypoxia-inducible genes, including vascular endothelial growth factor (VEGF), platelet-derived growth factor, transforming growth factor, glucose transporter 1, and phosphofructokinase-1.

The VHL/hypoxia-inducible factor pathway is believed to play a key role in the pathogenesis of VHL-related tumors (8). The excessive uncontrolled angiogenesis contributes to the hypervascular nature of tumors that develop in this condition. Furthermore, the pathogenic *VHL* gene may also result in abnormal regulation of the p53 tumor suppressor gene, nuclear factor-kB, retinol-binding protein 1, large subunit of ribonucleic acid (RNA) polymerase complex II, p400 chromatin-remodeling factor, and so on. The lack of a functional *VHL* gene can also lead to dysregulation of the extracellular matrix and microtubule cytoskeleton. All of the events previously mentioned may contribute to tumor formation in VHL.

VHL Diagnosis

VHL is associated with multiple tumors affecting various organs (Table 1). A VHL diagnosis can be made clinically when the characteristic clinical history and findings have manifested (8). The clinical diagnosis of VHL can be made in the following circumstances: *(a)* in a patient with a family history of VHL and at least one of the characteristic VHL-related tumors (eg, retinal HBs, CNS HBs, clear cell RCCs, pancreatic NETs, and endolymphatic sac tumors); *(b)* in the presence of two or more retinal or CNS HBs; or *(c)* in the presence of one retinal or CNS HB, plus at least one of the characteristic VHL-related visceral tumors, excluding renal and epididymal cysts.

Genetic testing for heterozygous germline *VHL* mutations may also confirm the diagnosis. Current indications for genetic testing include *(a)* patients with a suspected clinical diagnosis of VHL; *(b)* patients with close relatives in an established VHL family; and *(c)* patients with

Table 1: VHL Manifestations

Retina
Retinal HBs
CNS
Cerebellar and spinal HBs
Head and neck
Endolymphatic sac tumors
Pancreas
Pancreatic cysts
Serous cystadenomas
Pancreatic NETs
Kidney
Renal cysts
Clear cell RCCs
Adrenal gland
Pheochromocytoma
Reproductive organs
Epididymal cysts
Papillary cystadenoma of epididymis
Broad ligament cystadenoma

moderate suspicion for VHL who do not satisfy all criteria for a clinical diagnosis, which would include simplex cases with one retinal or CNS HB, a pheochromocytoma, or an endolymphatic sac tumor; the presence of at least two of the following tumors: a pancreatic cystadenoma, pancreatic NET, or epididymal papillary cystadenoma; or the presence of clear cell RCC, plus any of the following features: age less than 50 years, family history of clear cell RCC in a close relative, or bilateral/multifocal tumors (8).

Clinical Classification and Genotype-Phenotype Correlations

VHL is classified as type 1, 2A, 2B, or 2C on the basis of clinical phenotypes. Such phenotypic classifications have been shown to correlate with specific genotypic expressions (9–14). Patients with VHL type 1 are characterized as low risk for pheochromocytoma (9) but have an increased prevalence of retinal and CNS HBs, RCCs, pancreatic cysts, and NETs. Truncating mutations and exon deletions have been associated with type 1. Some authorities have proposed a type 1B, in which a patient has low risk for both pheochromocytoma and RCC. These patients have large *VHL* gene deletions involving *C3orf10* (9).

Patients with VHL type 2 harbor missense mutations and carry a high risk for pheochromocytoma (9–13). VHL type 2 is further classified into type 2A (high risk for pheochromocytoma and low risk for RCC), type 2B (high risk for pheochromocytoma and RCC), and type 2C (high risk for pheochromocytoma only). Although such genotype-phenotype correlations are promising for patient management, it should be noted that they are still evolving. As such, all patients with VHL should be screened for all possible VHL-related tumors, irrespective of their genotypic characteristics (8,14).

Retinal HBs

Retinal HBs, also called *retinal angiomas* or *capillary hemangiomas*, may develop in 45%–60% of VHL cases (7,15). The mean age of onset is 25 years (range, 1–68 years). Bilateral involvement may manifest in 50% of cases (16). Occasionally, these may be the sole manifestation of VHL.

The majority of these lesions occur in the peripheral retina (85%) (16). Retinal HBs may result in various complications such as macular exudation, exudative or tractional retinal detachment, vitreous hemorrhage, neovascular glaucoma, and vision loss. Factors associated with poor visual outcome include young age of onset, the manifestation of juxtapapillary lesions, an increase in both the number and extent of peripheral retina lesions, and the presence of missense or protein truncating mutations (16). Retinal HBs may result in blindness in 6% of cases.

The characteristic histologic findings of retinal HBs include fenestrated endothelial cells, pericytes, and lipid-rich foamy stromal cells. Immunohistochemical analysis has shown the presence of VEGF in the vacuolated stromal cells, which implies that these cells may represent the true neoplastic component of these lesions (17).

The diagnosis is confirmed with a comprehensive ophthalmic examination. Ophthalmoscopy may show a vascular tumor with dilated tortuous feeding vessels and optic disc edema. Fluorescein angiography, fundus photography, and optical coherence tomography may also be useful to monitor for new lesions and associated complications.

The role of imaging is limited, but magnetic resonance (MR) imaging of the brain or orbit may show a tiny enhancing retinal nodule, with or without retinal detachment (Fig 2). Treatment options include observation (for small asymptomatic lesions in the peripheral retina), argon laser photocoagulation, cryotherapy, photodynamic therapy, proton-beam radiation therapy, and surgical excision (18).

CNS HB

A CNS HB is the prototype tumor of VHL, which may occur in the cerebellum, brainstem, spinal cord, cauda equina, or supratentorial region (Figs 3–7). Craniospinal HB is the most common VHL-associated tumor, with a reported frequency of 60%–80% (4,7,8,15). CNS HB is commonly multifocal, with one study reporting multiple CNS HBs in 79% of 167 cases of VHL (19).

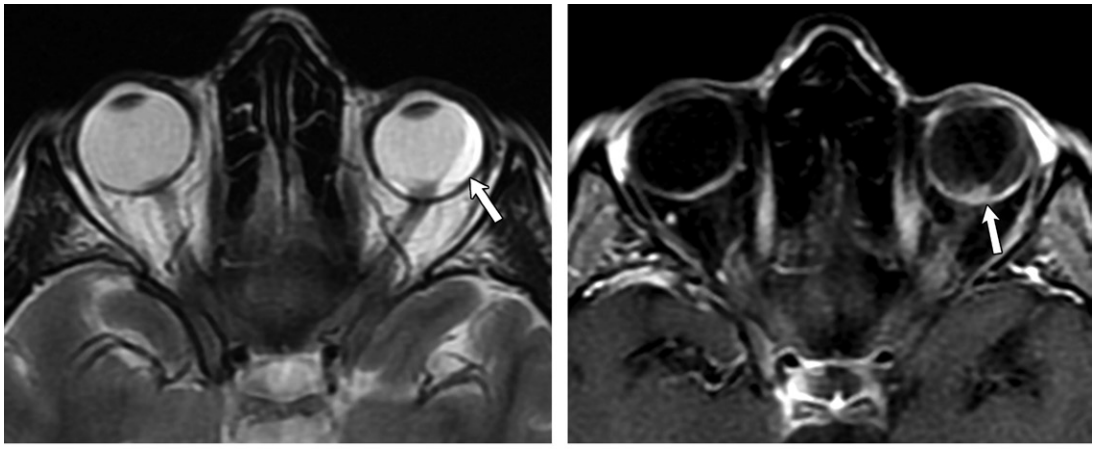

a. b.

Figure 2. Retinal HB in a 34-year-old woman with VHL. **(a)** Axial T2-weighted MR image of the orbit shows retinal detachment, with fluid in the subretinal space (arrow). **(b)** Axial contrast material–enhanced T1-weighted MR image shows a 7-mm enhancing lesion in the retina (arrow).

In VHL, CNS HBs most commonly occur in the cerebellum (44%–72%), followed by the spinal cord and brainstem (4,7,8,15). The mean age of onset is 33 years (range, 9–78 years). Patients with cerebellar HB may develop gait ataxia, dysmetria, headaches, diplopia, vertigo, and emesis (20,21). It should be noted that in many patients, the symptoms may be caused by the cyst or syrinx associated with the tumor rather than the tumor itself (19–21) (Fig 3). This is because tumor-related cysts/syrinxes grow at a much faster pace than the primary tumor and are typically larger than the tumor (19). Rarely, patients may develop spontaneous intracranial hemorrhage. Historically, cerebellar HBs have been classified into four subtypes (22,23): type 1 (5%) is a simple cyst without a macroscopic nodule; type 2 (60%) is a cyst associated with a mural nodule (Fig 3); type 3 (26%) is a solid tumor (Fig 4); and type 4 (9%) is a solid tumor with small internal cysts (22,23).

Some authors have also hypothesized that cerebellar HBs may begin as nodules, and those that remain solid may stay asymptomatic, while those that develop enlarging cysts may develop symptoms during the course of the disease (24). Macroscopically, CNS HBs are well-circumscribed yellow solid masses or mural nodules associated with fluid-filled cysts. CNS HBs are classified as World Health Organization (WHO) grade 1 tumors. Histologic analysis reveals a vascular capillary network lined with hyperplastic endothelial cells, which are surrounded by pleomorphic vacuolated stromal cells with lipid-rich cytoplasm (Fig 5). A metastatic clear cell RCC may have a similar appearance, causing a diagnostic dilemma, but immunohistochemical analysis may help differentiate the two conditions (25).

Angiographic images show a highly vascular tumor with enlarged arteries and early draining veins. Computed tomographic (CT) images show a well-defined homogeneous cyst with an isoattenuating mural nodule on nonenhanced images (26). Contrast-enhanced CT images show an avidly enhancing mural nodule within the cyst (the so-called cyst with mural nodule appearance) (Table 2). MR imaging features mimic those at CT. The cystic component is T1 hypointense and T2 hyperintense, and the mural nodule is T1 hypointense and T2 isointense or hyperintense.

After intravenous injection of gadolinium contrast material, the nodules show hypervascular enhancement while no enhancement is seen in the cyst wall. When a cerebellar HB is identified, it is important to image the whole spinal cord, as lesions in the spinal cord frequently coexist with cerebellar lesions (4,21,27) (Fig 6). The differential diagnosis includes juvenile pilocytic astrocytoma, arachnoid cyst, metastases, and medulloblastoma.

Since many tumors show a saltatory growth pattern (a growth phase followed by a quiescent phase), close surveillance may be appropriate for asymptomatic lesions. Surgical resection is performed for the symptomatic tumors, which are usually tumors with large associated cysts and/or peritumoral edema. Radiation therapy has also been used, especially in patients with incomplete surgical resection.

Spinal HBs manifest in 13%–50% of cases of VHL. The mean age of onset is 33 years (range, 11–66 years). Although any part of the spinal canal can be affected, spinal HBs are more common in the thoracic and cervical cord. Radiculopathy- and myelopathy-associated symptoms predominate in spinal HB, including hyperesthesia, weakness, gait ataxia, hyperreflexia, pain, incontinence, and rarely quadriplegia (21). Patients with a brainstem HB may develop symptoms due

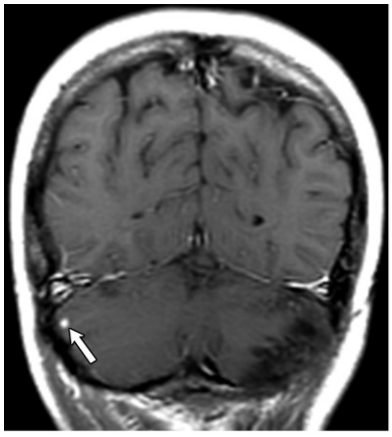

Figure 3. Cerebellar HB in a 32-year-old woman with VHL. **(a)** Coronal MR image of the brain obtained in 2003 shows a tiny solid enhancing nodule (arrow) in the right cerebellum. No cystic component is seen with the tumor. The tumor was monitored, as the patient was asymptomatic, and the lesion showed slow growth up til 2012. **(b)** Coronal MR image of the brain obtained in 2013 shows a slight increase in nodule size and a newly developed cystic component (arrow). The patient was still asymptomatic and was closely monitored. **(c)** Coronal MR image of the brain obtained in 2016 shows that the solid component has not changed much, but the cystic component (arrow) has significantly increased. **(d)** Axial T2-weighted MR image obtained in 2016 shows the large cystic lesion with mural nodule (arrow). Extensive peritumoral edema and mass effect from the enlarging cystic tumor are seen. The patient developed symptoms, and the tumor was successfully resected. Small solid nodules are usually asymptomatic, as in this case, while cystic lesions, especially those increasing in size and associated with peritumoral edema, often result in substantial symptoms that necessitate resection.

a.

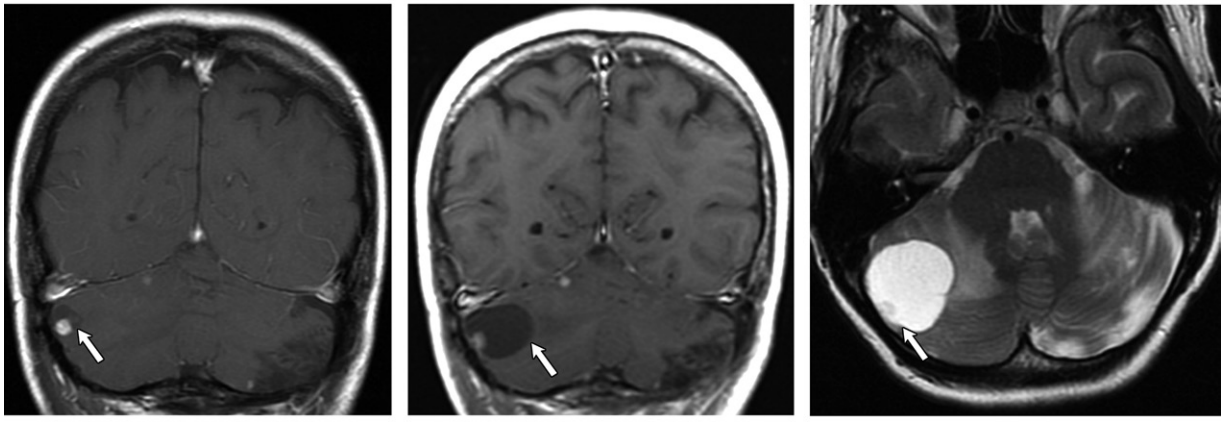

b. c. d.

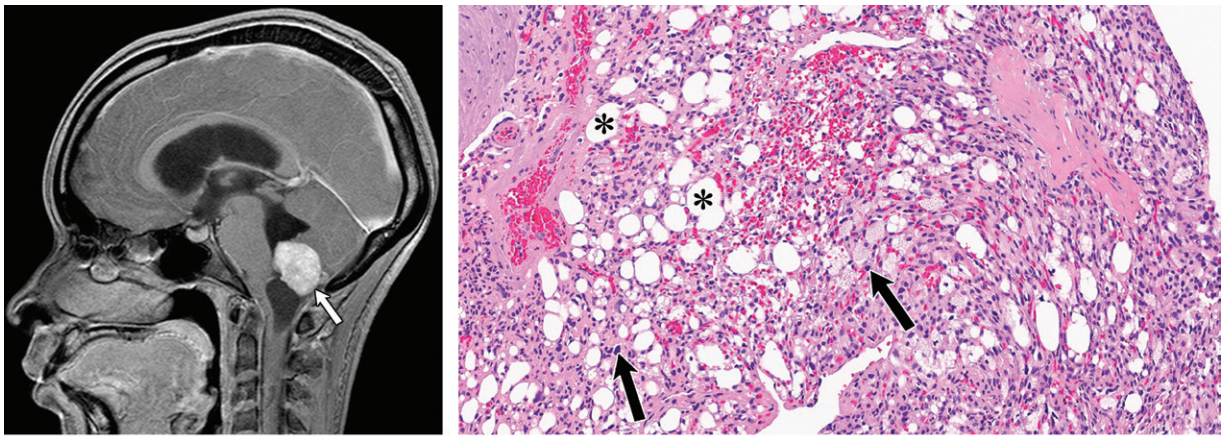

4. 5.

Figures 4, 5. **(4)** Cerebellar HB in a 28-year-old man with VHL. Sagittal contrast-enhanced T1-weighted MR image of the brain shows an avidly enhancing solid mass (arrow) in the posterior fossa. The appearance is consistent with type 3 cerebellar HB. Surgical pathologic analysis confirmed cerebellar HB. **(5)** Histopathologic findings of CNS HB. Photomicrograph shows proliferation of densely packed variably sized capillaries (*) with intervening polygonal stromal cells, some of which have foamy cytoplasm with fine vacuoles (arrows). (Hematoxylin-eosin [H-E] stain; original magnification, ×200.)

to lower cranial nerve compression and increased intracranial pressure (19–21).

A nonenhanced CT image may show an isoattenuating nodule in the spinal cord. Avid enhancement is seen in the spinal mass after intravenous contrast agent administration (Fig 7). MR imaging helps confirm an intramedullary tumor with an extramedullary component. The tumor nodule tends to be TI hypointense and T2 hyperintense and may show flow voids. Marked enhancement is seen on enhanced images. A syrinx is seen in 50%–100% of cases. The differential diagnosis includes metastasis, ependymoma, meningioma, arteriovenous

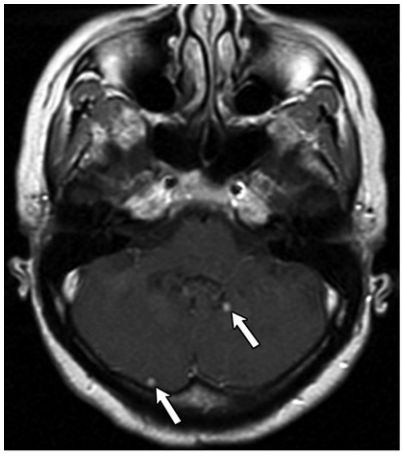


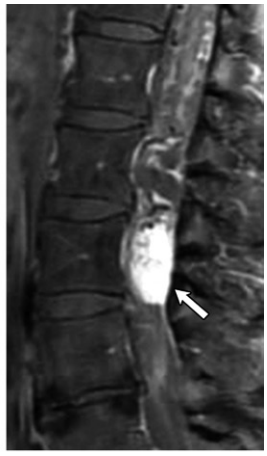

6a. 6b. 7a. 7b.

Figures 6, 7. **(6)** Multiple cerebellar and spinal HBs in a 38-year-old man with VHL. **(a)** Axial MR image of the brain shows small enhancing nodules (arrows) in the cerebellum, consistent with cerebellar HB. Although the patient did not have symptoms, MR imaging of the whole spine was performed. **(b)** Sagittal MR image of the cervical spine shows numerous tiny enhancing masses (arrows) in the spinal cord, consistent with spinal HB. **(7)** Spinal HB in a 27-year-old man with VHL. **(a)** Sagittal T1-weighted MR image of the lumbar spine demonstrates an isointense mass in the spinal cord (arrow). **(b)** Sagittal contrast-enhanced T1-weighted MR image of the lumbar spine demonstrates avid enhancement within the spinal cord mass (arrow).

Table 2: Imaging Features of VHL-related Benign and Malignant Tumors

Manifestations	Commonly Used Imaging Modalities*	Imaging Features
Cerebellar HB	MR imaging, CT	Well-defined homogeneous cyst with avidly enhancing mural nodule at CT and MR imaging; one-fourth of the tumors may manifest as a solid enhancing nodule, without cystic component
Spinal HB	MR imaging, CT	Avidly enhancing spinal mass, flow voids may be seen; syrinx seen in 50%–100% of cases
Endolymphatic sac tumor	MR imaging, CT	"Moth-eaten" appearance in the petrous temporal bone; central calcific spiculation and posterior rim calcification at CT; at MR imaging, these may be T1 hyperintense; intense enhancement of the solid portions of the tumor on gadolinium-enhanced images
Pancreatic cyst	MR imaging, CT	Simple-appearing thin-walled cysts without any mural nodules or enhancement
Serous cystadenoma	MR imaging, CT	Multicystic lesion with "bunch-of-grapes appearance"; tends to have multiple (usually more than six) cysts, with each one measuring <2 cm; enhancing central scar with stellate calcification (20%) may be seen; no communication with pancreatic duct
Pancreatic NET	MR imaging, CT	Lesions <3 cm tend to be solid and homogeneous; larger lesions are typically heterogeneous; avid early arterial enhancement at both CT and MR imaging; hypervascular liver metastases are often seen, especially in pancreatic tumors that are >3 cm
Renal cyst	MR imaging, CT	Simple-appearing thin-walled cysts without any mural nodules, nodular septa, or enhancement
Clear cell RCC	MR imaging, CT	Heterogeneous enhancing renal mass, typically as a hypervascular mass, which enhances more than the adjacent cortex; necrosis and calcification may be seen
Pheochromocytoma	MR imaging, CT, MIBG	Typically solid but can be cystic; avid arterial enhancement; marked T2 hyperintensity ("light bulb" sign) at MR imaging; avid tracer uptake on MIBG images
Papillary cystadenoma of epididymis	US	Mixed solid-cystic lesions, usually vascular with increased Doppler US flow; tend to be slow-growing lesions

*In VHL, MR imaging is usually preferred over CT for imaging tumors, as patients require long-term surveillance.
MIBG = metaiodobenzylguanidine, US = ultrasonography.

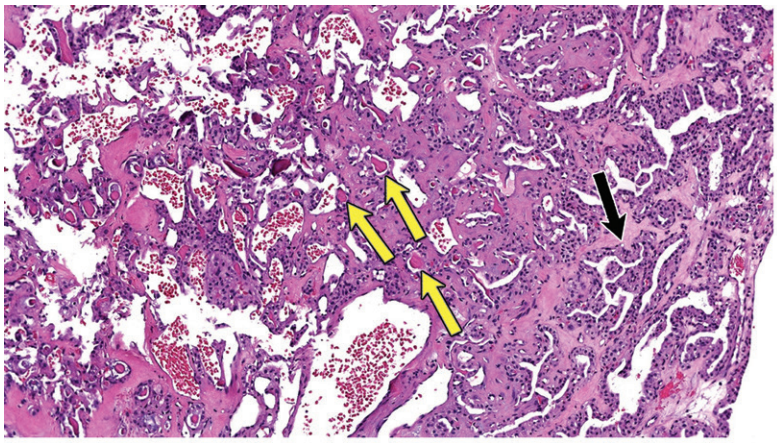

8.

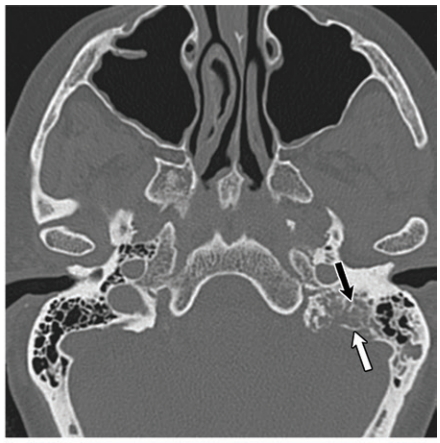

9.

Figures 8, 9. **(8)** Histopathologic findings of endolymphatic sac tumor. Photomicrograph shows a papillary partly cystic tumor lined by cuboidal to low columnar cells with eosinophilic cytoplasm (black arrow). The cysts vary in size, and some contain eosinophilic colloid-like material resembling thyroid follicles (yellow arrows). (H-E stain; original magnification, ×100.) **(9)** Endolymphatic sac tumor in a 34-year-old woman with VHL. Axial high-resolution CT image of the petrous temporal bone shows an infiltrative aggressive mass (white arrow) in the retrolabyrinthine region, resulting in a moth-eaten appearance. The tumor contains intratumoral bone spicules (black arrow).

malformation, or arteriovenous fistula. Surgical resection and γ-knife radiation therapy may be offered as treatment options in the management of these tumors.

Endolymphatic Sac Tumor

Endolymphatic sac tumor develops in 10%–15% of VHL cases (Figs 8–10). The mean age of onset is 22 years (range, 12–50 years), and they may be bilateral in 30% of cases (28,29). These are benign tumors that occur in the vestibular aqueduct but are locally invasive and can erode into the adjacent structures such as the semicircular canals and cochlea. Clinical symptoms include hearing loss (84%–100%), tinnitus (73%–77%), vertigo (62%–68%), and facial nerve palsy (8%) (28–30). Hearing loss may be sudden (secondary to intralabyrinthine hemorrhage) or gradual (usually owing to endolymphatic hydrops) (28). Histopathologic analysis shows a highly vascular tumor, comprised of complex interdigitating papillary cystic structures lined with cuboidal epithelium, infiltrating the surrounding connective tissue and bone (Fig 8) (4). Hemorrhage, hemosiderin, cholesterol clefts, and clear vacuolated cells are seen.

At CT, endolymphatic sac tumors may demonstrate a moth-eaten appearance in the petrous temporal bone, with erosive changes in the vestibular aqueduct, semicircular canals, and cochlea (31,32) (Fig 9). Central calcific spiculation and posterior rim calcification are commonly seen (31,32). Enhanced images show an avidly enhancing tumor.

At MR imaging, these tumors may be T1 hyperintense (secondary to hemorrhagic and proteinaceous contents) and T2 hyperintense (31,32). Intense enhancement of the solid portions of the tumor is seen on gadolinium-enhanced images (Fig 10). Accurate early diagnosis of endolymphatic sac tumors followed by prompt surgical resection is critical, as they can help prevent or reduce hearing loss and other audiovestibular symptoms (30).

Renal Manifestations

Multicentric renal cysts and clear cell RCCs may manifest in more than two-thirds of VHL cases (15) (Figs 11–16). Even grossly normal renal parenchyma may demonstrate hundreds of microscopic renal cysts and tumors (33). The cystic lesions may be a combination of simple benign cysts, complex atypical cysts with epithelial hyperplasia/cytologic atypia, or cystic RCCs (34) (Figs 11–13). The number and size of the cysts in VHL have not been shown to be associated with malignant potential (34). Patients may be asymptomatic despite the manifestation of a large number of cysts.

VHL is characterized by the development of a clear cell RCC histologic subtype (4,14,27). The prevalence of RCC in VHL varies from 25% to 45%, with the frequency increasing with age (4,8,15). VHL-related RCCs tend to develop at a much younger age compared with that of sporadic RCCs. The mean age of onset for VHL-related RCCs is 39 years (range, 13–70 years), and clear cell RCCs are frequently bilateral (Figs 12–14). It should be noted that bilateral clear cell RCCs on their own are not diagnostic of VHL, as other hereditary renal tumor syndromes and rarely even sporadic tumors may manifest as bilateral multifocal tumors (8).

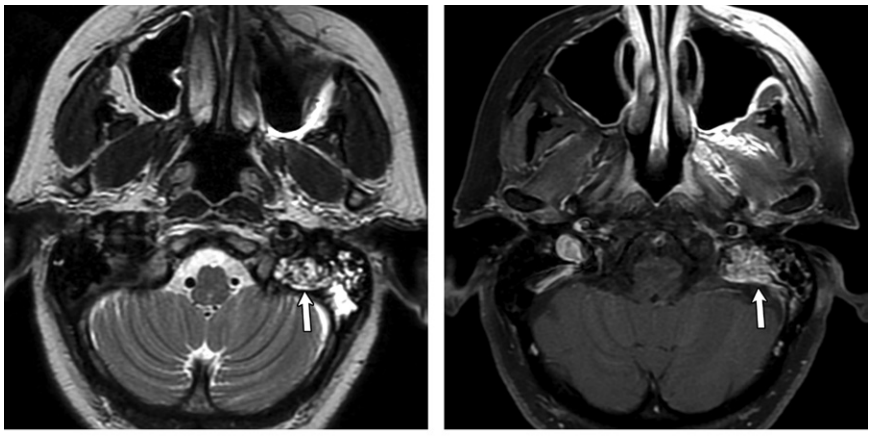

Figure 10. Endolymphatic sac tumor in a 44-year-old woman with VHL. **(a)** Axial T2-weighted MR image of the petrous temporal bone shows a heterogeneous hyperintense mass (arrow) in the left retrolabyrinthine region. **(b)** Axial contrast-enhanced T1-weighted MR image shows avid enhancement in the mass (arrow).

a. **b.**

11. **12.**

Figures 11, 12. **(11)** Diffuse bilateral renal cysts in a 34-year-old man with VHL. Coronal T2-weighted image of the abdomen shows diffuse bilateral hyperintense cysts in both kidneys. **(12)** RCC and renal cyst in a 41-year-old man with VHL. Coronal contrast-enhanced T1-weighted MR image shows bilateral cystic lesions with thick septa (white arrow), a solid heterogeneous enhancing left renal mass (black arrow), and a simple right renal cyst (arrowhead).

However, the presence of bilateral or multifocal clear cell RCCs or tumors in patients younger than 50 years of age is an indication for VHL genetic screening (Fig 12).

Gross pathologic analysis of a solid RCC shows a well-defined encapsulated gold-yellow-tan variegated mass, which may demonstrate cystic degeneration and hemorrhage. Histopathologic analysis demonstrates nests of epithelial cells with clear cytoplasm and well-defined cell membranes, separated by highly vascularized stroma (Fig 15).

Ultrasonography (US) may help differentiate solid from cystic renal masses. Although contrast-enhanced US is promising, its use for assessing complex renal lesions in VHL is not yet clear. Currently, renal lesions are usually further evaluated at CT or MR imaging. Renal protocol CT with nonenhanced, corticomedullary, nephrographic, and occasionally excretory phase imaging is useful for characterizing renal lesions.

At CT, solid RCCs tend to be heterogeneous and demonstrate early avid enhancement, followed by washout in the delayed phase (Fig 1). At MR imaging, solid RCCs tend to be T1 hypointense, although the presence of hemorrhage may result in T1 hyperintense foci. The presence of intracellular lipid in clear cell RCCs may rarely result in signal loss with out-of-phase chemical shift MR imaging sequences. Tumors are typically T2 hyperintense and demonstrate avid heterogeneous enhancement (Figs 12, 13, 16). Cystic RCCs may manifest as cysts with enhancing solid components and/or thick nodular septa (Fig 12). In contrast, simple renal cysts are homogeneously T1 hypointense and T2 hyperintense and lack enhancement on dynamic contrast-enhanced images.

MR imaging is increasingly used to monitor VHL, as it offers several advantages compared with CT. MR imaging is not associated with any radiation exposure, which makes it an attractive

Figures 13–15. **(13)** Bilateral RCCs in a 32-year-old man. Axial contrast-enhanced T1-weighted MR image of the abdomen shows numerous bilateral heterogeneously enhancing lesions (arrows) in both kidneys. Given the presence of bilateral multifocal clear cell RCCs in a young patient, the appearance raised concern for VHL. The diagnosis was confirmed with genetic testing. **(14)** Bilateral RCCs in a 42-year-old man with VHL. Coronal contrast-enhanced MR image of the abdomen demonstrates hypervascular heterogeneous bilateral renal masses (arrows). Surgical clips are also seen in the left suprarenal region, consistent with a history of left adrenalectomy for pheochromocytoma. The larger 4-cm mass in the interpolar region of the left kidney was chosen for partial nephrectomy, while the other lesions (which were <3 cm) were closely monitored. **(15)** Photomicrograph of clear cell RCC shows nests of tumor cells with delicate vascular patterns (arrows). The cells have clear cytoplasm and low-grade nuclei. (H-E stain; original magnification, ×100.)

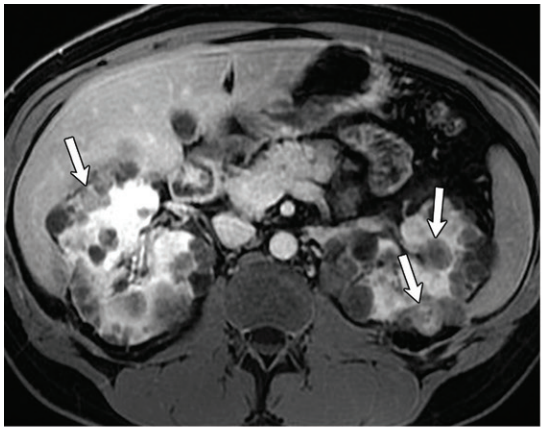

13.

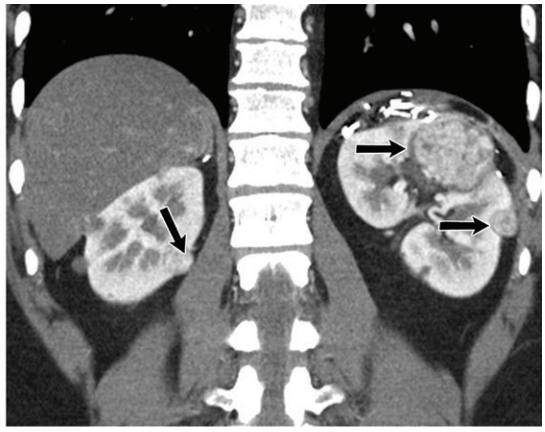

14.

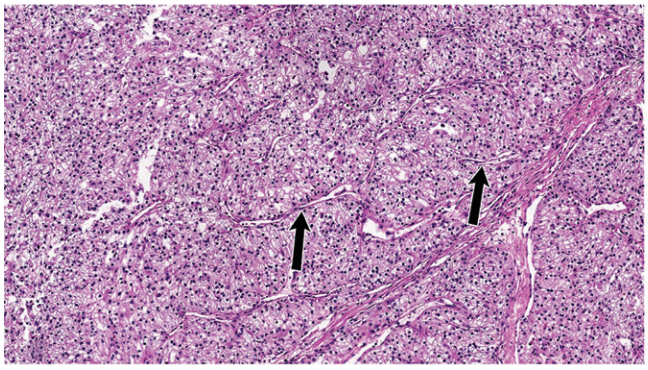

15.

tool, as long-term surveillance is required for VHL patients. Furthermore, many patients with VHL may have renal impairment owing to prior renal surgery and therefore may not be able to receive intravenous contrast agents. In these circumstances, nonenhanced MR imaging provides a much better assessment of VHL-related tumors compared with that of nonenhanced CT.

In addition, MR imaging can be useful for patients with an allergy to iodinated intravenous contrast agents. Finally, MR imaging may be superior to CT for evaluating renal lesions, especially smaller lesions. Small renal cysts, particularly those that are less than a centimeter, are difficult to evaluate at CT owing to the phenomenon of pseudoenhancement, which makes it challenging to differentiate the cysts from small RCCs (35). This pitfall can be overcome with MR imaging.

Traditionally, RCCs associated with VHL were treated with radical nephrectomies. This approach mandated the need for renal replacement therapies such as dialysis or transplantation, which are associated with reduced functional outcome and quality of life. However, studies have clearly shown that partial nephrectomies are associated with significantly higher cancer-free survival rates at 5 and 10 years compared with those of radical nephrectomies, and they have now become the standard of care (36,37). Furthermore, the need for dialysis is reported to be low, even after multiple partial nephrectomies, implying that these nephron-sparing surgeries offer both superior oncologic and functional outcomes compared with those of radical nephrectomies (36,37).

Several studies have evaluated the growth kinetics of RCC in VHL, and the results have been variable. Choyke et al (38) reported that VHL-associated RCCs may grow at a rate of 0.2–2.2 cm/year, with a mean growth rate of 1.6 cm/year. Another study involving 64 VHL cases with 96 renal tumors reported a mean growth rate of 0.4

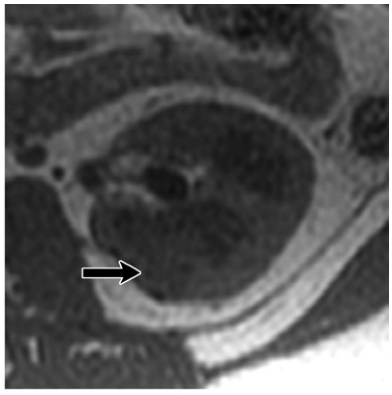

a.

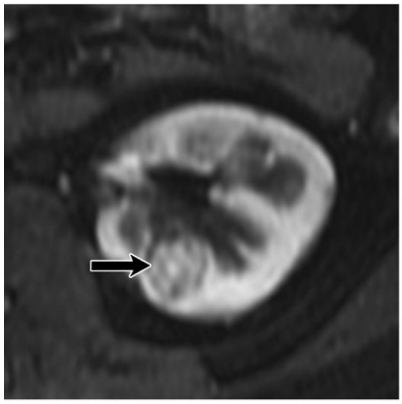

b.

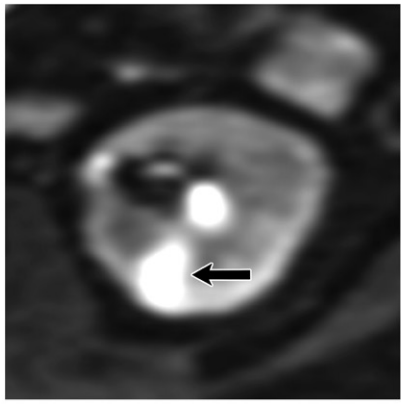

c.

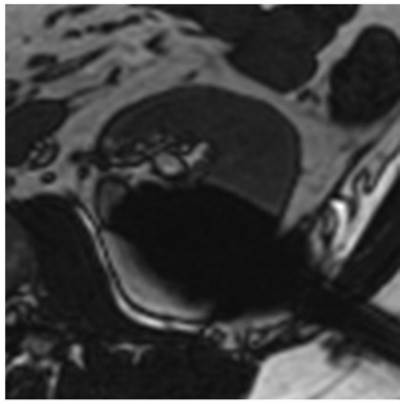

d.

Figure 16. RCC in a 46-year-old woman with VHL who underwent right radical nephrectomy 10 years earlier, as well as partial nephrectomy in the left kidney 3 years earlier. **(a, b)** Axial nonenhanced T1-weighted **(a)** and contrast-enhanced T1-weighted **(b)** MR images of the left kidney show a hypervascular enhancing solid mass (arrow) in the left kidney. **(c)** Axial high *b*-value diffusion-weighted MR image shows restricted diffusion in the lesion (arrow). The patient underwent cryoablation of the left RCC. **(d)** Axial T2-weighted MR image shows a cryoprobe, causing cryoablation of the left renal mass.

cm/year and a mean volume doubling time of 26 months (39). Many health care centers use a tumor larger than 3 cm as the cutoff for a partial nephrectomy, as the metastatic potential below this size has been shown to be exceedingly low (40,41). However, it should be noted that there is a high risk of de novo recurrent tumors in VHL, and the need for repeat partial nephrectomies may be as high as 63%–85% (37,42). Therefore, some authors have proposed a 4-cm cutoff size for surgery, as this might help to delay the time to surgery and also potentially decrease the number of repeat surgeries, thereby reducing complication rates (43).

Image-guided ablative procedures such as radiofrequency ablation and cryoablation may play an important role in the management of VHL-related RCCs. Noncystic RCCs measuring 2–3 cm have been successfully treated with ablative procedures, with studies reporting up to a 100% 5-year cancer-specific survival rate (44–46) (Fig 16). However, cystic RCCs and tumors closely related to major abdominal structures are contraindications for ablative procedures (46). Furthermore, the recurrence rates may be higher after ablative procedures compared with those of partial nephrectomies, and therefore, these patients require continued close monitoring (44–46).

There was a paradigm shift in the management of metastatic RCCs after the advent of targeted therapy. Numerous tyrosine kinase agents have been approved by the U.S. Food and Drug Administration for metastatic RCCs, such as sorafenib, sunitinib, pazopanib, and axitinib. Although the number of studies that have evaluated these drugs in VHL-associated RCCs is small, the initial results have been promising, and further studies are currently under investigation (47,48).

Pancreatic Manifestations

Patients with VHL can develop pancreatic cysts, serous cystadenomas, and pancreatic NETs (4,14,27) (Figs 17–22). Pancreatic cysts are common in VHL and may be seen in 42% of cases (range, 7%–72%) (Fig 17) (49). These are typically multiple and usually asymptomatic. Interestingly, pancreatic cysts may be the only manifestation in about 12% of patients at the time of initial VHL diagnosis (49).

Serous cystadenomas occur in 11% of patients (range, 9%–17%) (49–51). At histopathologic analysis, serous cystadenomas demonstrate well-demarcated multilocular clusters of small cysts, separated by thin fibrous septa. These cystic lesions are lined by cuboidal cells, without mucin or papillary structures. Both pancreatic cysts and serous cystadenomas tend to be asymptomatic,

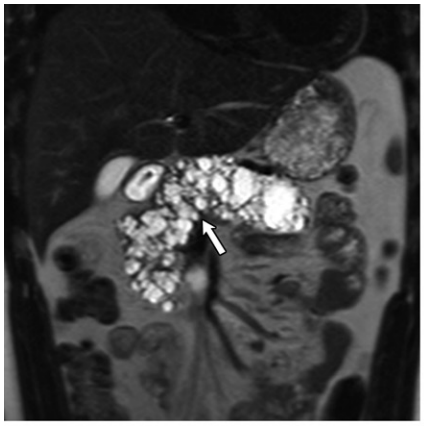

17.

Figures 17, 18. **(17)** Pancreatic cysts in a 42-year-old man with VHL. Coronal T2-weighted MR image of the abdomen shows the entire pancreas replaced by innumerable pancreatic cysts (arrow). Although pancreatic cysts are usually asymptomatic, they may result in pancreatic insufficiency when they are extensive and replace the entire pancreas, as seen in this case. **(18)** Serous cystadenoma, pancreatic cysts, and pancreatic NET in a 39-year-old man with VHL. Axial contrast-enhanced CT image **(a)** and axial T2-weighted MR image **(b)** of the abdomen show a cluster of cysts with a central enhancing scar (white arrow) in the tail of the pancreas. These cysts have a characteristic bunch of grapes appearance, with multiple cysts (more than six), with each cyst measuring less than 2 cm, consistent with serous cystoadenoma. There is an avidly enhancing solid mass in the head of the pancreas (black arrow), consistent with an NET. There are also large pancreatic cysts (arrowhead).

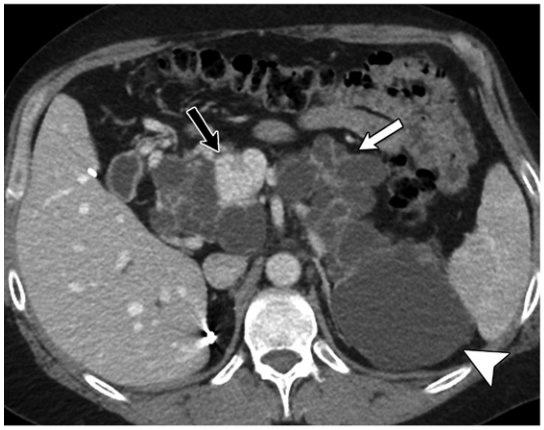

18a.

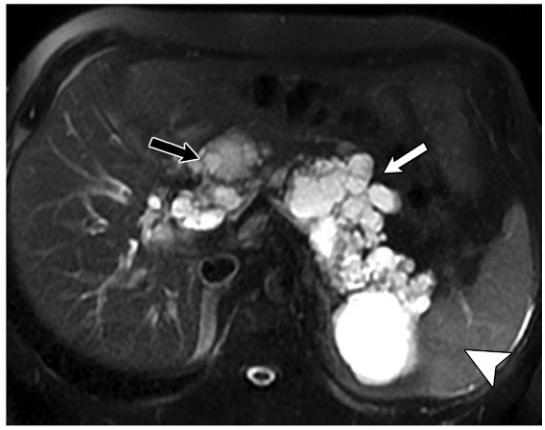

18b.

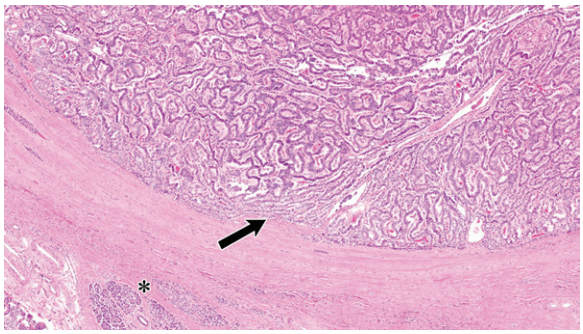

Figure 19. Histopathologic findings of a pancreatic NET. Photomicrograph shows a tumor, characterized by a trabecular pattern (arrow) and low-grade cytologic features. Adjacent normal pancreatic acini (*) can also be seen. (H-E stain; original magnification, ×20.)

but larger lesions may cause nonspecific abdominal pain, and extensive cystic lesions replacing most of the pancreas may result in pancreatic insufficiency and diabetes mellitus (52).

Imaging, especially CT and MR imaging, plays an important role in the evaluation of pancreatic lesions in VHL. At CT, pancreatic cysts are seen as hypoattenuating lesions with fluid attenuation and demonstrate no enhancement. Serous cystadenomas occur as lobulated multilocular septated cystic masses. CT images show a multicystic lesion with the characteristic bunch of grapes appearance (Fig 18). These benign cystic lesions have multiple cysts (usually more than six), and each cyst measures less than 2 cm. An enhancing central scar with stellate calcification (20% of cases) may be seen.

MR imaging shows a T1 hypointense and T2 hyperintense "cluster of cysts." The central fibrotic scar may be hypointense on both T1- and T2-weighted images and can demonstrate delayed enhancement. Serous cystadenomas do not communicate with the pancreatic duct, which helps differentiate them from intraductal papillary mucinous neoplasms. When multiple simple pancreatic cysts are closely apposed to each other, it may be difficult to distinguish them from serous cystadenomas. However, this differentiation may not be clinically relevant, as both are benign lesions, requiring no treatment unless symptomatic.

Pancreatic NETs develop in 15% of patients with VHL (range, 9%–17%) (49). The mean age of onset is 35 years, but NETs have been reported in patients as young as 13 years of age. About 53% of VHL-associated pancreatic NETs are multiple. Although any part of the pancreas may be involved, they are more common in the head and uncinate process of the pancreas.

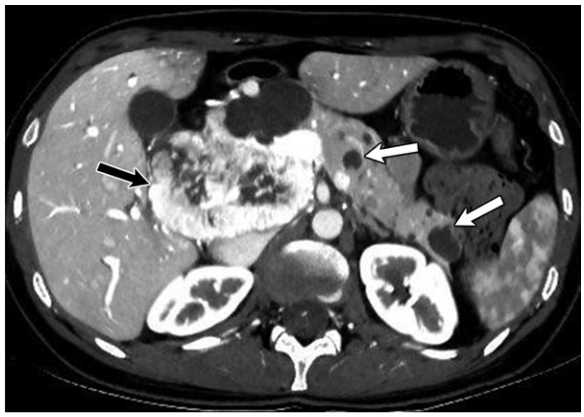

20.

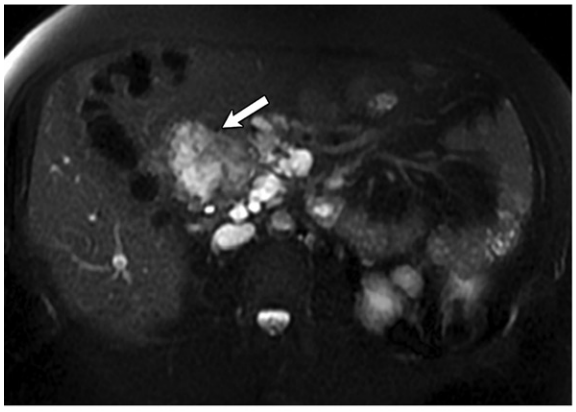

21a.

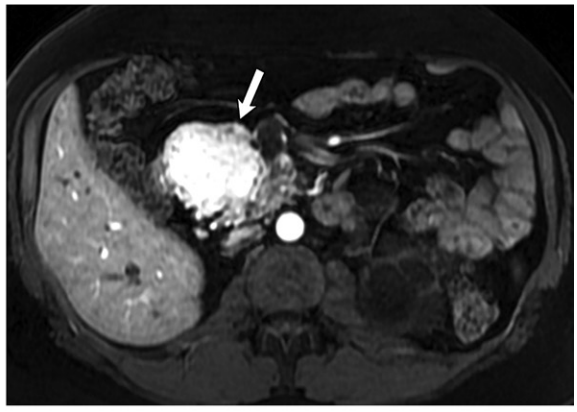

21b.

Figures 20, 21. **(20)** Pancreatic NET and pancreatic cysts in a 36-year-old man with VHL. Axial contrast-enhanced MR image of the abdomen shows a markedly hypervascular heterogeneous mass (black arrow) in the head of the pancreas, consistent with an NET. Numerous scattered nonenhancing cysts are also seen in the pancreas (white arrows). **(21)** Pancreatic NET in a 42-year-old woman with VHL. **(a)** Axial T2-weighted MR image of the abdomen shows a heterogeneous hyperintense tumor (arrow) in the head of the pancreas. **(b)** Axial arterial phase gadolinium-enhanced T1-weighted MR image shows avid enhancement within the tumor (arrow).

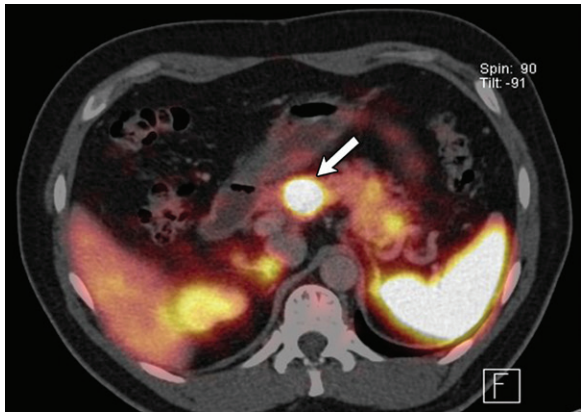

Figure 22. Pancreatic NET in a 43-year-old man. Axial gallium 68 (^{68}Ga) 1,4,7,10-tetraazacyclododecane-1,4,7,10-tetraacetic acid (DOTA)–octreotate (DOTATATE) positron emission tomography (PET)/CT image shows avid tracer uptake in the tumor (arrow) in the body of the pancreas.

Pancreatic NETs associated with VHL manifest at a much younger age compared with that of sporadic NETs, and they are more commonly multifocal. The vast majority of these pancreatic NETs are nonfunctional tumors (50,51).

Although they tend to be asymptomatic, some NETs may result in abdominal pain, jaundice, pancreatitis, or even gastrointestinal bleeding (50). At gross pathologic analysis, these tumors are well circumscribed and are red-brown, gray, or yellow-tan (53,54). Solid trabecular or glandular architecture, with prominent small vasculature and stromal collagen bands, is commonly seen at histopathologic analysis (Fig 19). A characteristic feature of pancreatic NETs associated with VHL is the presence of clear cells and multivacuolated lipid-rich cells (53,54). At immunohistochemical analysis, these tumors are usually positive for synaptophysin, chromogranin A, inhibin, neuron-specific enolase, and S100.

Tumors may also demonstrate focal positivity for pancreatic polypeptide, somatostatin, insulin, and/or glucagon (53,54). The manifestations of angioinvasion, perineural invasion, and peritumoral fat infiltration are signs of locally aggressive tumors and may be associated with poor prognosis (53). The incidence of malignancy in VHL-associated pancreatic NETs varies from 8% to 13%, with tumors demonstrating local invasion and regional or distant metastases (49,55). Pancreatic NETs associated with VHL are classified pathologically, as per the WHO classification, based on the tumor mitoses per 10 high-power fields and the Ki-67 index (53).

Pancreatic NETs are usually hypoattenuating or isointense on nonenhanced CT images. The

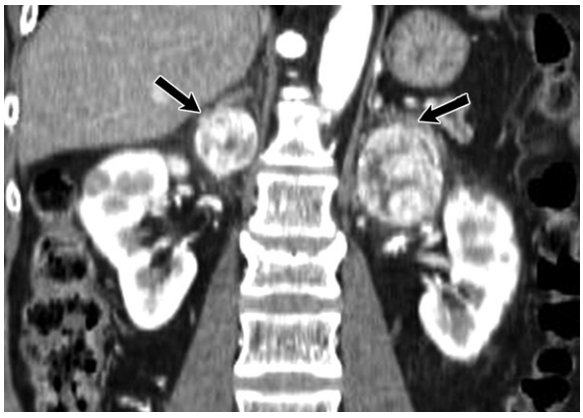

Figure 23. Bilateral pheochromocytomas in a 22-year-old man with VHL. Coronal contrast-enhanced CT image of the abdomen shows heterogeneous avidly enhancing bilateral adrenal masses (arrows). Biochemical tests revealed elevated levels of plasma metanephrines, consistent with pheochromocytoma.

lesions demonstrate intense early arterial enhancement (Fig 20). Typically, small lesions less than 3 cm are solid and homogeneous. Tumors greater than 3 cm may be heterogeneous. It is important that a proper pancreatic CT protocol is used for evaluating these tumors, as a poor CT technique may lead to missed diagnosis.

At MR imaging, pancreatic NETs are T1 hypointense and T2 hyperintense (Fig 21). The enhancement pattern mimics that which is seen at CT (avid arterial enhancement with washout on delayed phase images). In most patients with VHL, the diagnosis of pancreatic NETs is often made with imaging alone. However, when there is a diagnostic dilemma, endoscopic US and biopsy may be useful for confirming the diagnosis. Hepatic metastases may be seen in pancreatic NETs, especially in pancreatic tumors less than 3 cm. The liver metastases also tend to be hypervascular, similar to the primary tumor. Upper abdominal nodal metastases may also be seen. Distant metastases may also develop at other sites.

Fluorine 18 (^{18}F) fluorodeoxyglucose (FDG) PET/CT has been reported to be useful in the management of pancreatic NETs (56–58). Although CT and MR imaging may allow identification of more NETs compared with those identified at ^{18}F-FDG PET/CT, the latter may demonstrate extra lesions that can be occult at CT or MR imaging, implying that combined multimodality imaging using anatomic and functional imaging may be helpful in these patients (58).

Furthermore, ^{18}F-FDG PET/CT may be helpful for prognostication. Pancreatic NETs with high total lesion glycolysis at PET/CT are reported to be high-grade tumors, with higher malignant/metastatic potential compared with those with low total lesion glycolysis (56). Recent studies evaluating the clinical use of ^{68}Ga-DOTA-TATE PET/CT and ^{68}Ga-DOTA-NaI^{3}-octreotide PET/CT in pancreatic NETs have shown promising early results (59,60) (Fig 22).

Considering that less than 20% of pancreatic NETs associated with VHL are malignant, a conservative approach with a "watch-and-wait" strategy is an important part of the management of these tumors. Studies have shown that about 40% of NETs in VHL may be stable or even decrease in size. Surgical resection may be appropriate for pancreatic NETs in VHL when the tumor size is greater than 3 cm (or >2 cm for lesions in the head of the pancreas), the tumor doubling time is less than 500 days, there is a mutation in exon 3, or there is suspicion of regional nodal metastases (51,61).

Smaller tumors that are stable or display slow growth may be closely monitored with annual CT or MR imaging. Intraoperative US may help identify lesions that may be occult at CT; it can also demonstrate the relationship of the tumor to the pancreatic duct, an important feature that can guide the surgical approach (49). Closer follow-up imaging is warranted after surgical resection, especially for higher-grade tumors. CT and MR imaging may be performed every 3–6 months for the 1st year after resection and every 6 months for the 2nd year, with annual follow-up thereafter (51).

Pheochromocytoma

Adrenal pheochromocytomas may develop in 25%–30% of VHL cases (62,63). The mean age of onset is 27 years (range, 5–58 years). VHL-associated pheochromocytomas manifest more commonly in boys (63), and 20%–50% may be bilateral (62,63) (Fig 23). The risk of developing a second tumor increases with age, with studies reporting a 50% risk of a second tumor at 30 years after the initial diagnosis (63); 1%–5% of these tumors are malignant (63).

Extra-adrenal pheochromocytomas/paragangliomas may be seen in 15% of VHL cases at various sites along the sympathetic chain in the abdomen, thorax, or head and neck. Patients may be asymptomatic or experience classic symptoms such as paroxysmal or refractory hypertension, palpitations, headaches, sweating, and hypertensive crises (62). A diagnosis of a pheochromocytoma is usually confirmed on the basis of biochemical abnormalities, including elevated plasma metanephrine and 24-hour urinary catecholamine levels (64).

At gross pathologic analysis, pheochromocytomas manifest as lobulated yellow-red-brown tumors with a thick vascular tumor capsule. Histopathologic analysis shows a characteristic nesting microscopic pattern, including well-defined small round tumor cells with eosinophilic and clear cytoplasm, separated by vascular hyalinized stroma (Fig 24). Cystic degeneration,

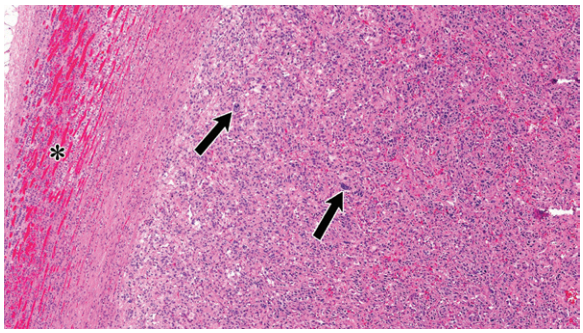

Figure 24. Histopathologic findings of a pheochromocytoma. Photomicrograph shows tumor cells arranged in small nests with a rich vascular network. Occasional cells with marked pleomorphism (arrows) are also seen. Normal adrenal cortical tissue is visualized at the periphery (*). (H-E stain; original magnification, ×40.)

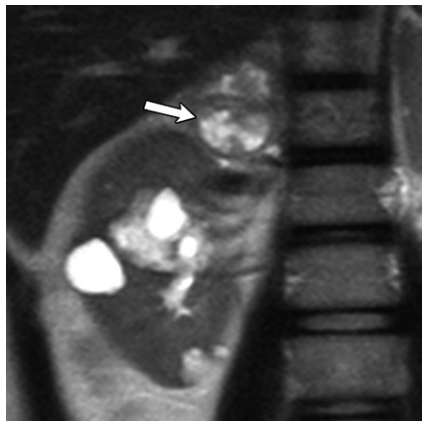

Figure 25. Pheochromocytoma in a 34-year-old woman with VHL. Coronal T2-weighted MR image of the abdomen shows heterogeneous high signal intensity in a right adrenal mass (arrow). Since the patient was symptomatic, the tumor was resected. Surgical pathologic analysis confirmed pheochromocytoma.

necrosis, calcification, lipid accumulation, and fibrosis may be seen.

At CT, most tumors are solid heterogeneous lesions, but lesions may also be cystic. Pheochromocytomas typically show avid arterial enhancement (Fig 23) (65). However, even adenomas and hypervascular adrenal metastases may show similar enhancement characteristics (66). Absolute and relative percentage CT washout values of pheochromocytomas and adrenal adenomas may overlap (66,67). Therefore, CT enhancement characteristics may not necessarily help diagnose a pheochromocytoma (64).

High T2-weighted signal intensity (similar to cerebrospinal fluid signal intensity) within the adrenal mass is a useful imaging feature for diagnosing pheochromocytoma (Fig 25) (66). Schieda et al (66) reported that a quantitative adrenal-to-muscle signal intensity ratio of 3.95 or greater on T2-weighted images was 88% specific and 81% sensitive for pheochromocytomas.

Radionuclide imaging, such as iodine 131 (^{131}I) or ^{123}I metaiodobenzylguanidine (MIBG) scintigraphy, may also be useful in imaging pheochromocytoma for tumor localization and detecting occult metastatic disease (Fig 26). However, while MIBG has a high specificity for pheochromocytoma, it has a relatively low sensitivity, and therefore a negative image does not exclude the diagnosis of pheochromocytoma (64). Recent studies indicate that PET/CT, especially ^{68}Ga-DOTATATE PET/CT, may be more sensitive than ^{131}I-MIBG scintigraphy for localizing metastatic pheochromocytoma (68,69).

Minimally invasive, adrenal cortical–sparing surgical resection is currently preferred for managing these tumors (70). Given the high risk of recurrence and developing second de novo tumors (20%–50%), surveillance with imaging and biochemical tests is important (63,71).

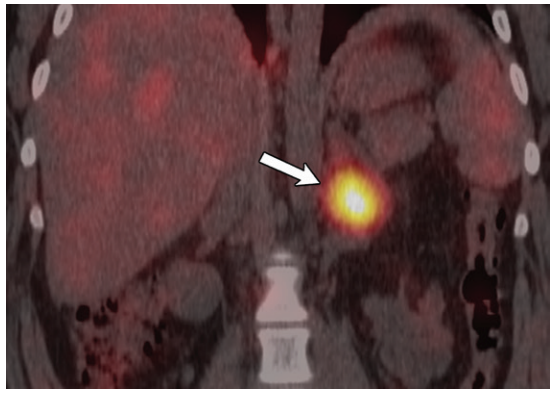

Figure 26. Pheochromocytoma in an 18-year-old woman with VHL. Coronal ^{123}I MIBG image shows avid uptake of MIBG in a left adrenal mass (arrow), consistent with pheochromocytoma.

Manifestations in the Reproductive Organs

Papillary cystadenomas are the most common VHL-related tumors developing in the reproductive organs, occurring predominantly in the epididymis in men but may rarely develop in the broad ligament and mesosalpinx in women.

Epididymal papillary cystadenomas develop in 25%–60% of patients with VHL (Fig 27) (8,72,73), usually seen in young men, 20–40 years of age. Bilateral epididymal papillary cystadenomas should raise strong suspicion for VHL, as 60% of bilateral tumors occur in VHL (72). Epididymal papillary cystadenomas arise from the efferent ductules of the epididymis (72). They are small tumors ranging from 1 to 4 cm. These are usually solid tumors with cystic spaces filled with colloid material but may be predominantly cystic, with small papillae that are lined by glycogen-rich clear cells (72).

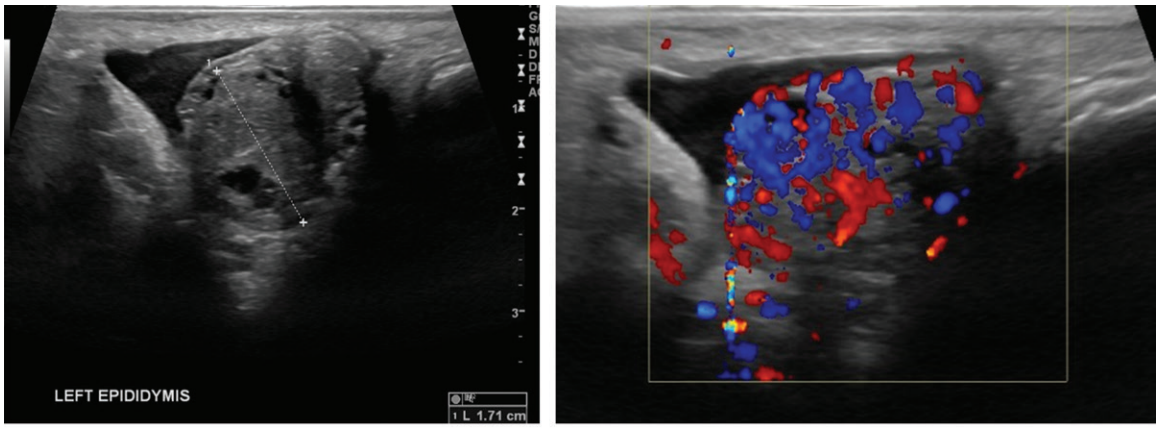

a. b.

Figure 27. Epididymal papillary cystadenoma in a 31-year-old man with VHL. **(a)** Gray-scale US image of the left epididymis shows a mixed solid cystic mass in the head of the left epididymis. **(b)** Color Doppler US image shows marked vascularity with increased Doppler flow seen within the left epididymal mass. The patient was asymptomatic. The lesion was monitored with US follow-ups and demonstrated minimal growth.

Patients are usually asymptomatic but may present with incidentally identified scrotal masses. US appearances mimic the pathologic findings and range from cystic masses containing solid components to predominantly solid masses in the epididymis (27,73). These are usually vascular tumors demonstrating increased Doppler flow (Fig 27). Dilated efferent testicular ductules may manifest.

Some authors have proposed the following US criteria for diagnosing epididymal cystadenomas in VHL: *(a)* a predominantly solid epididymal mass larger than 14 × 10 mm; *(b)* occurring in a patient with known VHL; and *(c)* a lesion that shows slow growth (73,74). These are benign tumors and are typically managed conservatively.

Rarely, papillary cystadenomas may manifest in the broad ligament in women (4,7,16,24). The histologic appearance of these tumors resembles that of the epididymal papillary cystadenomas. Being benign lesions, these are usually managed conservatively, but surgical resection may be considered if symptomatic (4,7,16).

VHL Surveillance

Surveillance forms an extremely important component in the management of VHL and has been shown to increase the life expectancy (5). Various national guidelines exist for VHL surveillance, including those proposed by the VHL Alliance, the Dutch VHL guidelines, and the Danish VHL Coordination Group guidelines (75–77). VHL Alliance surveillance guidelines, which are commonly followed in the United States, suggest that surveillance should start at birth and continue lifelong (Table 3). Special precautions may be required during pregnancy.

Conclusion

VHL is a familial cancer syndrome caused by a mutation in the *VHL* tumor suppressor gene, mapped on human chromosome 3p25. Patients with VHL are at risk for developing numerous benign and malignant tumors that affect multiple organs. While some of the VHL-related manifestations such as renal and pancreatic cysts are frequently asymptomatic, other manifestations such as retinal and CNS HBs, RCCs, pheochromocytomas, and pancreatic NETs may be associated with significant morbidity and mortality. Early detection plays a key role in the optimal management of this condition. Radiologists should be aware of the imaging features of the various tumors that can occur in VHL. Familiarity with the current recommendations for VHL surveillance is also important, as these patients require lifelong follow-up.

Acknowledgment.—We would like to thank Kelly Kage for preparing the images.

Disclosures of Conflicts of Interest.—**M.G.L.** *Activities related to the present article:* disclosed no relevant relationships. *Activities not related to the present article:* grants from Ethicon and Philips. *Other activities:* disclosed no relevant relationships. **P.J.P.** *Activities related to the present article:* disclosed no relevant relationships. *Activities not related to the present article:* consultant for Bracco and Check Cap; royalties from Elsevier; and stock in Elucent, SHINE, Cellectar, and VirtuoCTC. *Other activities:* disclosed no relevant relationships.

References

1. Maher ER, Iselius L, Yates JR, et al. Von Hippel-Lindau disease: a genetic study. J Med Genet 1991;28(7):443–447.
2. Neumann HP, Wiestler OD. Clustering of features of von Hippel-Lindau syndrome: evidence for a complex genetic locus. Lancet 1991;337(8749):1052–1054.
3. Richards FM, Payne SJ, Zbar B, Affara NA, Ferguson-Smith MA, Maher ER. Molecular analysis of de novo germline mutations in the von Hippel-Lindau disease gene. Hum Mol Genet 1995;4(11):2139–2143.

Table 3: VHL Alliance Surveillance Recommendations

Age	Surveillance Recommendations
At birth	Clinical evaluation for neurologic disturbance, ophthalmic examination, and newborn hearing tests
1–4 years of age	Annual comprehensive ophthalmic examination Annual clinical evaluation for neurologic disturbances and abnormalities in blood pressure, vision, and hearing
5–15 years of age	All of the surveillance recommendations at birth and at ages 1–4 Annual biochemical tests, including plasma metanephrine or 24-hour urinary metanephrine levels Annual abdominal US from 8 years of age or earlier if indicated; MR imaging of the abdomen or functional imaging with MIBG scintigraphy to be performed only if biochemical abnormalities are found Audiology assessment every 2–3 years (annually if any audiovestibular symptoms) MR imaging with contrast enhancement of the internal auditory canal every 2–3 years
≥16 years of age	Annual comprehensive ophthalmic examination Annual clinical evaluation for neurologic disturbances and abnormalities in blood pressure, vision, and hearing Annual biochemical tests, including plasma metanephrine or 24-hour urinary metanephrine levels Annual abdominal US and abdominal MR imaging with and without contrast enhancement every 1–2 years Annual MR imaging with and without contrast enhancement of the brain, petrous temporal bone, and whole spine every 2–3 years
Pregnancy	Regular eye examination (risk of rapid progression of retinal HB) MR imaging of the brain and whole spine without contrast enhancement (to ensure that there is no rapid progression or complications such as hydrocephalus) Plasma metanephrine levels in early, mid-, and late pregnancy to test for active pheochromocytoma Consider cesarean delivery if patient has known retinal or CNS tumors

Source.—Reference 77.

4. Lonser RR, Glenn GM, Walther M, et al. Von Hippel-Lindau disease. Lancet 2003;361(9374):2059–2067.
5. Wilding A, Ingham SL, Lalloo F, et al. Life expectancy in hereditary cancer predisposing diseases: an observational study. J Med Genet 2012;49(4):264–269.
6. Nordstrom-O'Brien M, van der Luijt RB, van Rooijen E, et al. Genetic analysis of von Hippel-Lindau disease. Hum Mutat 2010;31(5):521–537.
7. Chittiboina P, Lonser RR. Von Hippel-Lindau disease. Handb Clin Neurol 2015;132:139–156.
8. Nielsen SM, Rhodes L, Blanco I, et al. Von Hippel-Lindau disease: genetics and tole of genetic counseling in a multiple neoplasia syndrome. J Clin Oncol 2016;34(18):2172–2181.
9. McNeill A, Rattenberry E, Barber R, Killick P, MacDonald F, Maher ER. Genotype-phenotype correlations in VHL exon deletions. Am J Med Genet A 2009;149A(10):2147–2151.
10. Maranchie JK, Afonso A, Albert PS, et al. Solid renal tumor severity in von Hippel Lindau disease is related to germline deletion length and location. Hum Mutat 2004;23(1):40–46.
11. Hes F, Zewald R, Peeters T, et al. Genotype-phenotype correlations in families with deletions in the von Hippel-Lindau (VHL) gene. Hum Genet 2000;106(4):425–431.
12. Maher ER, Webster AR, Richards FM, et al. Phenotypic expression in von Hippel-Lindau disease: correlations with germline VHL gene mutations. J Med Genet 1996;33(4):328–332.
13. Chen F, Kishida T, Yao M, et al. Germline mutations in the von Hippel-Lindau disease tumor suppressor gene: correlations with phenotype. Hum Mutat 1995;5(1):66–75.
14. Frantzen C, Klasson TD, Links TP, Giles RH. Von Hippel-Lindau syndrome. In: Pagon RA, Adam MP, Ardinger HH, et al, eds. GeneReviews. Seattle, Wash: University of Washington, 1993. https://www.ncbi.nlm.nih.gov/books/NBK1463/. Updated August 6, 2015. Accessed May 15, 2017.
15. Maher ER, Yates JR, Harries R, et al. Clinical features and natural history of von Hippel-Lindau disease. Q J Med 1990;77(283):1151–1163.
16. Wong WT, Agrón E, Coleman HR, et al. Clinical characterization of retinal capillary hemangioblastomas in a large population of patients with von Hippel-Lindau disease. Ophthalmology 2008;115(1):181–188.
17. Chan CC, Vortmeyer AO, Chew EY, et al. VHL gene deletion and enhanced VEGF gene expression detected in the stromal cells of retinal angioma. Arch Ophthalmol 1999;117(5):625–630.
18. Chew EY. Ocular manifestations of von Hippel-Lindau disease: clinical and genetic investigations. Trans Am Ophthalmol Soc 2005;103:495–511.
19. Wanebo JE, Lonser RR, Glenn GM, Oldfield EH. The natural history of hemangioblastomas of the central nervous system in patients with von Hippel-Lindau disease. J Neurosurg 2003;98(1):82–94.
20. Kanno H, Kobayashi N, Nakanowatari S. Pathological and clinical features and management of central nervous system hemangioblastomas in von Hippel-Lindau disease. J Kidney Cancer VHL 2014;1(4):46–55.
21. Lonser RR, Butman JA, Huntoon K, et al. Prospective natural history study of central nervous system hemangioblastomas in von Hippel-Lindau disease. J Neurosurg 2014;120(5):1055–1062.
22. Richard S, Campello C, Taillandier L, Parker F, Resche F. Haemangioblastoma of the central nervous system in von Hippel-Lindau disease: French VHL Study Group. J Intern Med 1998;243(6):547–553.

23. Lee SR, Sanches J, Mark AS, Dillon WP, Norman D, Newton TH. Posterior fossa hemangioblastomas: MR imaging. Radiology 1989;171(2):463–468.
24. Slater A, Moore NR, Huson SM. The natural history of cerebellar hemangioblastomas in von Hippel-Lindau disease. AJNR Am J Neuroradiol 2003;24(8):1570–1574.
25. Rivera AL, Takei H, Zhai J, Shen SS, Ro JY, Powell SZ. Useful immunohistochemical markers in differentiating hemangioblastoma versus metastatic renal cell carcinoma. Neuropathology 2010;30(6):580–585.
26. Leung RS, Biswas SV, Duncan M, Rankin S. Imaging features of von Hippel-Lindau disease. RadioGraphics 2008;28(1):65–79; quiz 323.
27. Choyke PL, Glenn GM, Walther MM, Patronas NJ, Linehan WM, Zbar B. von Hippel-Lindau disease: genetic, clinical, and imaging features. Radiology 1995;194(3):629–642.
28. Butman JA, Kim HJ, Baggenstos M, et al. Mechanisms of morbid hearing loss associated with tumors of the endolymphatic sac in von Hippel-Lindau disease. JAMA 2007;298(1):41–48.
29. Manski TJ, Heffner DK, Glenn GM, et al. Endolymphatic sac tumors: a source of morbid hearing loss in von Hippel-Lindau disease. JAMA 1997;277(18):1461–1466.
30. Kim HJ, Hagan M, Butman JA, et al. Surgical resection of endolymphatic sac tumors in von Hippel-Lindau disease: findings, results, and indications. Laryngoscope 2013;123(2):477–483.
31. Patel NP, Wiggins RH 3rd, Shelton C. The radiologic diagnosis of endolymphatic sac tumors. Laryngoscope 2006;116(1):40–46.
32. Mukherji SK, Albernaz VS, Lo WW, et al. Papillary endolymphatic sac tumors: CT, MR imaging, and angiographic findings in 20 patients. Radiology 1997;202(3):801–808.
33. Walther MM, Lubensky IA, Venzon D, Zbar B, Linehan WM. Prevalence of microscopic lesions in grossly normal renal parenchyma from patients with von Hippel-Lindau disease, sporadic renal cell carcinoma and no renal disease: clinical implications. J Urol 1995;154(6):2010–2014; discussion 2014–2015.
34. Solomon D, Schwartz A. Renal pathology in von Hippel-Lindau disease. Hum Pathol 1988;19(9):1072–1079.
35. Tappouni R, Kissane J, Sarwani N, Lehman EB. Pseudoenhancement of renal cysts: influence of lesion size, lesion location, slice thickness, and number of MDCT detectors. AJR Am J Roentgenol 2012;198(1):133–137.
36. Singer EA, Vourganti S, Lin KY, et al. Outcomes of patients with surgically treated bilateral renal masses and a minimum of 10 years of followup. J Urol 2012;188(6):2084–2088.
37. Steinbach F, Novick AC, Zincke H, et al. Treatment of renal cell carcinoma in von Hippel-Lindau disease: a multicenter study. J Urol 1995;153(6):1812–1816.
38. Choyke PL, Glenn GM, Walther MM, et al. The natural history of renal lesions in von Hippel-Lindau disease: a serial CT study in 28 patients. AJR Am J Roentgenol 1992;159(6):1229–1234.
39. Jilg CA, Neumann HP, Gläsker S, et al. Growth kinetics in von Hippel-Lindau-associated renal cell carcinoma. Urol Int 2012;88(1):71–78.
40. Walther MM, Choyke PL, Glenn G, et al. Renal cancer in families with hereditary renal cancer: prospective analysis of a tumor size threshold for renal parenchymal sparing surgery. J Urol 1999;161(5):1475–1479.
41. Duffey BG, Choyke PL, Glenn G, et al. The relationship between renal tumor size and metastases in patients with von Hippel-Lindau disease. J Urol 2004;172(1):63–65.
42. Ploussard G, Droupy S, Ferlicot S, et al. Local recurrence after nephron-sparing surgery in von Hippel-Lindau disease. Urology 2007;70(3):435–439.
43. Jilg CA, Neumann HP, Gläsker S, et al. Nephron sparing surgery in von Hippel-Lindau associated renal cell carcinoma: clinicopathological long-term follow-up. Fam Cancer 2012;11(3):387–394.
44. Yang B, Autorino R, Remer EM, et al. Probe ablation as salvage therapy for renal tumors in von Hippel-Lindau patients: the Cleveland Clinic experience with 3 years follow-up. Urol Oncol 2013;31(5):686–692.
45. Park BK, Kim CK. Percutaneous radio frequency ablation of renal tumors in patients with von Hippel-Lindau disease: preliminary results. J Urol 2010;183(5):1703–1707.
46. Matin SF, Ahrar K, Wood CG, Daniels M, Jonasch E. Patterns of intervention for renal lesions in von Hippel-Lindau disease. BJU Int 2008;102(8):940–945.
47. NIH U.S. National Library of Medicine. Pazopanib in von Hippel-Lindau (VHL) syndrome. https://clinicaltrials.gov/ct2/show/NCT01436227. Published September 19, 2011. Accessed May 15, 2017.
48. Jonasch E, McCutcheon IE, Waguespack SG, et al. Pilot trial of sunitinib therapy in patients with von Hippel-Lindau disease. Ann Oncol 2011;22(12):2661–2666.
49. Charlesworth M, Verbeke CS, Falk GA, Walsh M, Smith AM, Morris-Stiff G. Pancreatic lesions in von Hippel-Lindau disease? A systematic review and meta-synthesis of the literature. J Gastrointest Surg 2012;16(7):1422–1428.
50. Hammel PR, Vilgrain V, Terris B, et al. Pancreatic involvement in von Hippel-Lindau disease: the Groupe Francophone d'Etude de la Maladie de von Hippel-Lindau. Gastroenterology 2000;119(4):1087–1095.
51. Keutgen XM, Hammel P, Choyke PL, Libutti SK, Jonasch E, Kebebew E. Evaluation and management of pancreatic lesions in patients with von Hippel-Lindau disease. Nat Rev Clin Oncol 2016;13(9):537–549.
52. Mukhopadhyay B, Sahdev A, Monson JP, Besser GM, Reznek RH, Chew SL. Pancreatic lesions in von Hippel-Lindau disease. Clin Endocrinol (Oxf) 2002;57(5):603–608.
53. Cassol C, Mete O. Endocrine manifestations of von Hippel-Lindau disease. Arch Pathol Lab Med 2015;139(2):263–268.
54. Lubensky IA, Pack S, Ault D, et al. Multiple neuroendocrine tumors of the pancreas in von Hippel-Lindau disease patients: histopathological and molecular genetic analysis. Am J Pathol 1998;153(1):223–231.
55. Igarashi H, Ito T, Nishimori I, et al. Pancreatic involvement in Japanese patients with von Hippel-Lindau disease: results of a nationwide survey. J Gastroenterol 2014;49(3):511–516.
56. Satoh K, Sadowski SM, Dieckmann W, et al. (18)F-FDG PET/CT volumetric parameters are associated with tumor grade and metastasis in pancreatic neuroendocrine tumors in von Hippel-Lindau disease. Ann Surg Oncol 2016;23(suppl 5):714–721.
57. Sadowski SM, Weisbrod AB, Ellis R, et al. Prospective evaluation of the clinical utility of 18-fluorodeoxyglucose PET CT scanning in patients with von Hippel-Lindau-associated pancreatic lesions. J Am Coll Surg 2014;218(5):997–1003.
58. Kitano M, Millo C, Rahbari R, et al. Comparison of 6-18F-fluoro-L-DOPA, 18F-2-deoxy-D-glucose, CT, and MRI in patients with pancreatic neuroendocrine neoplasms with von Hippel-Lindau disease. Surgery 2011;150(6):1122–1128.
59. Prasad V, Tiling N, Denecke T, Brenner W, Plöckinger U. Potential role of (68)Ga-DOTATOC PET/CT in screening for pancreatic neuroendocrine tumour in patients with von Hippel-Lindau disease. Eur J Nucl Med Mol Imaging 2016;43(11):2014–2020.
60. Krausz Y, Freedman N, Rubinstein R, et al. 68Ga-DOTA-NOC PET/CT imaging of neuroendocrine tumors: comparison with ^{111}In-DTPA-octreotide (OctreoScan®). Mol Imaging Biol 2011;13(3):583–593.
61. Blansfield JA, Choyke L, Morita SY, et al. Clinical, genetic and radiographic analysis of 108 patients with von Hippel-Lindau disease (VHL) manifested by pancreatic neuroendocrine tumors (PNETs). Surgery 2007;142(6):814–818; discussion 818.e1–818.e2.
62. Aufforth RD, Ramakant P, Sadowski SM, et al. Pheochromocytoma screening initiation and frequency in von Hippel-Lindau syndrome. J Clin Endocrinol Metab 2015;100(12):4498–4504.
63. Bausch B, Wellner U, Bausch D, et al. Long-term prognosis of patients with pediatric pheochromocytoma. Endocr Relat Cancer 2013;21(1):17–25.
64. Blake MA, Kalra MK, Maher MM, et al. Pheochromocytoma: an imaging chameleon. RadioGraphics 2004;24(suppl 1):S87–S99.
65. Northcutt BG, Raman SP, Long C, et al. MDCT of adrenal masses: can dual-phase enhancement patterns be used to differentiate adenoma and pheochromocytoma? AJR Am J Roentgenol 2013;201(4):834–839.
66. Schieda N, Alrashed A, Flood TA, Samji K, Shabana W, McInnes MD. Comparison of quantitative MRI and CT

washout analysis for differentiation of adrenal pheochromocytoma from adrenal adenoma. AJR Am J Roentgenol 2016;206(6):1141–1148.
67. Patel J, Davenport MS, Cohan RH, Caoili EM. Can established CT attenuation and washout criteria for adrenal adenoma accurately exclude pheochromocytoma? AJR Am J Roentgenol 2013;201(1):122–127.
68. Janssen I, Chen CC, Millo CM, et al. PET/CT comparing (68)Ga-DOTATATE and other radiopharmaceuticals and in comparison with CT/MRI for the localization of sporadic metastatic pheochromocytoma and paraganglioma. Eur J Nucl Med Mol Imaging 2016;43(10):1784–1791.
69. Tan TH, Hussein Z, Saad FF, Shuaib IL. Diagnostic performance of (68)Ga-DOTATATE PET/CT, (18)F-FDG PET/CT and (131)I-MIBG scintigraphy in mapping metastatic pheochromocytoma and paraganglioma. Nucl Med Mol Imaging 2015;49(2):143–151. [Published correction appears in Nucl Med Mol Imaging 2015;49(2):152.]
70. Baghai M, Thompson GB, Young WF Jr, Grant CS, Michels VV, van Heerden JA. Pheochromocytomas and paragangliomas in von Hippel-Lindau disease: a role for laparoscopic and cortical-sparing surgery. Arch Surg 2002;137(6):682–688; discussion 688–689.
71. Lee JE, Curley SA, Gagel RF, Evans DB, Hickey RC. Cortical-sparing adrenalectomy for patients with bilateral pheochromocytoma. Surgery 1996;120(6):1064–1070; discussion 1070–1071.
72. Odrzywolski KJ, Mukhopadhyay S. Papillary cystadenoma of the epididymis. Arch Pathol Lab Med 2010;134(4):630–633.
73. Choyke PL, Glenn GM, Wagner JP, et al. Epididymal cystadenomas in von Hippel-Lindau disease. Urology 1997;49(6):926–931.
74. Akbar SA, Sayyed TA, Jafri SZ, Hasteh F, Neill JS. Multimodality imaging of paratesticular neoplasms and their rare mimics. RadioGraphics 2003;23(6):1461–1476.
75. Binderup ML, Bisgaard ML, Harbud V, et al. Von Hippel-Lindau disease (vHL): national clinical guideline for diagnosis and surveillance in Denmark—3rd edition. Dan Med J 2013;60(12):B4763.
76. Kruizinga RC, Sluiter WJ, de Vries EG, et al. Calculating optimal surveillance for detection of von Hippel-Lindau-related manifestations. Endocr Relat Cancer 2013;21(1):63–71.
77. VHL Family Alliance. The VHL handbook: what you need to know about VHL—a reference handbook for people with von Hippel-Lindau disease, their families, and support personnel. CreateSpace (Amazon's independent publishing platform): Boston, Mass, 2014.

DW imaging in the chest are welcomed and do extend beyond what is reviewed in our article. In our practice, we do not routinely perform quantitative measurements of ADC for most thoracic lesions. The main purposes of DW imaging for our basic thoracic MR imaging protocols are to provide a heavily T2-weighted sequence at low *b* values as well as a means of qualitative assessment of diffusion restriction using higher *b* values and the ADC map. As understanding of the implications of DW imaging of the chest evolves, quantitative analysis of DW imaging may take on a greater role, but it is not essential or warranted at present for interpretation of most thoracic MR imaging examinations.

Regarding the second comment by Dr Priola and colleagues, pertaining to our use of thoracic MR imaging to determine whether a suspected lesion has properties that make it certainly or near certainly benign, this is our most common indication for thoracic MR imaging. As stated in our article, we did not intend to provide a comprehensive list of all potential indications for MR imaging of the chest, and we did not imply that the evaluation of whether a lesion is certainly or near certainly benign is the only indication for thoracic MR imaging. The indications listed by Dr Priola et al in their letter are newer niche first-line indications that are promising. We sincerely hope that these and other indications for thoracic MR imaging continue to grow and contribute to the expansion of thoracic MR imaging in clinical practice.

Constantine A. Raptis, MD, Sebastian R. McWilliams, MB BCh, BAO, Kristy L. Ratkowski, MD, Sanjeev Bhalla, MD, Mallinckrodt Institute of Radiology, 510 S. Kingshighway Blvd, Campus Box 8131, St Louis, MO 63110

Jordi Broncano, MD, Department of Radiology, Hospital Cruz Roja, Córdoba, Spain

Daniel B. Green, MD, Department of Radiology, Weill Medical College, New York–Presbyterian Hospital, New York, NY

e-mail: *raptisc@wustl.edu*

Erratum

Originally published online:

https://doi.org/10.1148/rg.2018170156

Tumors in von Hippel–Lindau Syndrome: From Head to Toe—Comprehensive State-of-the-Art Review

Dhakshinamoorthy Ganeshan, Christine O. Menias, Perry J. Pickhardt, Kumaresan Sandrasegaran, Meghan G. Lubner, Preetha Ramalingam, Sanjeev Bhalla

Erratum in:

RadioGraphics 2018;38(3):982 • https://doi.org/10.1148/rg.2018184005

Figure 23 legend: The legend should read as follows: "Bilateral pheochromocytomas in a 22-year-old man with VHL. Coronal contrast-enhanced CT image of the abdomen shows heterogeneous avidly enhancing bilateral **adrenal** [not renal] masses (arrows). Biochemical tests revealed elevated levels of plasma metanephrines, consistent with pheochromocytoma."